Study of the compounding process parameters for morphology control of LDPE/layered silicate nano-composites

Serena Coiai,[1] [2]* Marco Scatto,[1] Monica Bertoldo[3], Lucia Conzatti[4], Leonardo Andreotti[1], Marion Sterner[1], Elisa Passaglia[5], Giovanna Costa[4],Francesco Ciardelli[2,3]

[1]Centro Italiano Packaging (CIP), Via delle Industrie 25/8, 30175 Venezia, Italy; Fax: +39 041 5093648; e-mail: marco.scatto@centroitalianopackaging.com

[2]*Department of Chemistry and Industrial Chemistry, University of Pisa, Via Risorgimento 35, 56126 Pisa, Italy, Fax: +39 050 2219320; e-mail: serena.coiai@ns.dcci.unipi.it;

[3]PolyLab-CNR c/o Department of Chemistry and Industrial Chemistry, University of Pisa, Via Risorgimento 35, 56126 Pisa, Italy.

[4]ISMAC-CNR, Genova Section, Area della Ricerca di Genova, Via E. De Marini 6, Genova, Italy.

[5]ICCOM-CNR Pisa section c/o Department of Chemistry and Industrial Chemistry, Via Risorgimento 35, 56126 Pisa, Italy.

Abstract: A careful insight into melt compounding procedure is proposed in order to achieve a better understanding and control of the dispersion and orientation mechanisms of organo-clay platelets into LDPE nanocomposites. The method involved is the preparation of a maleic anhydride grafted polyethylene master-batch containing 10 wt% organo-clay via twin-screw extrusion. A substantial nano-dispersion and orientation of clay platelets was obtained as observed by X-ray diffraction (XRD) and transmission electron microscopy (TEM) analyses. Moreover, the nanocomposites prepared by diluting the master-batch through the blend mixing with additional LDPE preserved or improved the exfoliation and lamellae orientation. Finally, the thermo-gravimetric analysis (TGA) showed a significant improvement of the thermal stability while both differential scanning calorimetry (DSC) and XRD evidenced a slight increase of the LDPE crystallinity degree with respect to neat polymer matrices thus suggesting the occurrence of orientation also for the polymer.

Introduction

In recent years, polymers filled with small amounts of high aspect ratio layered silicates, dispersed at nanoscale level, have been the subject of deep research efforts due to the possibility to obtain materials with improved properties and a broader application field [1-6]. Particularly interesting is its use as food packaging materials [7, 8] due to the excellent gas barrier properties that generally characterize the films from such nanocomposites jointly to improved flame retardancy, higher stiffness and toughness. For example, nanocomposites of this type from low density polyethylene (LDPE), which is widely used for packaging applications, show oxygen barrier properties significantly improved with transparency preservation.

A large number of papers were already published concerning the preparation of polyethylene (PE)/montmorillonite nanocomposites by melt processing routes [9-11]

and several aspects on their preparation [12-20] were deeply investigated for obtaining the best results in terms of clay exfoliation. It is in fact well known that to completely profit by all the advantages of nanocomposites it is necessary to achieve exfoliation or delamination of the large stacks of silicate nanoplatelets into single layers or small tactoids, thus achieving the enormous aspect ratio necessary to contribute to the nanocomposite property profile.

In this perspective many synthetic efforts were focused to design effective surfactants for clay modification, and for PE significant results were found by using organo-montmorillonite modified with quaternary ammonium salts having long alkyl chains. Moreover it was found that for establishing interactions between the clay and the polymer to be able to stabilize the final morphology it is necessary to introduce functional groups onto the polyolefin backbone and then to use the modified polymer either as matrix or as compatibilizer. In particular, it was shown that grafted maleic anhydride (MAH) or diethyl maleate groups [21, 22] promote effective hydrophilic interactions between the layered silicate surface and the polyolefin, thus providing good mechanical and gas barrier properties [21-23]. In particular, in the case of PE/organo-clay nanocomposites [18] the exfoliated morphology could be obtained with MAH grafting levels higher than 0,1 wt% and number of methylene groups in alkylamine chains more than 16. Furthermore, the dispersion level was found to strongly depend on the amount of silicate and the evolution of different morphologies from disordered exfoliated to predominantly intercalated was studied with respect to the organo-clay content [23]. High density polyethylene (HDPE) [14-16] and linear low density polyethylene (LLDPE) [17-19] were preferentially used for the preparation of nanocomposites since it was demonstrated that branched LDPE macromolecules hardly intercalate into clay galleries [20].

Melt viscosity and molecular weight play an important role in establishing the composite final morphology [24, 25]. The best results were obtained by using a compatibilizer with similar rheological properties with respect to the matrix; otherwise the miscibility between the two polymers can be compromised thus inhibiting and limiting the intercalation/exfoliation process.

Along with the use of a properly selected organic clay modifier and compatibilizer, a correct mixing protocol (processing parameters such as mean residence time, screw speed etc.), which promotes both high shear stress and high shear rate, can assist the clay dispersion [26-30]. Dennis et. al. [30] demonstrated that at the beginning of the melt compounding process the stress should help the breakup of larger organo-clay particles into dispersed stacks of silicate tactoids. Then the transfer of the stress from the molten polymer to the silicate tactoids shears them into smaller stacks of silicate platelets and ultimately individual platelets peel apart through a combination of shear and diffusion of polymer chains into the organo-clay galleries. However, this pathway does not require high shear intensity, but involves the polymer diffusion into the galleries (driven by either physical or chemical affinity of the polymer for the organo-clay surface) and thus it is facilitated by a high residence time in the extruder. Therefore, the model demonstrated that, without chemical interactions between the resin matrix and the clay, high shear intensity does not cause a further breakdown of the particles and only by combining chemistry and processing the delamination and dispersion can be improved.

A rapid and direct determination of the nanocomposite morphology during or at the end of the extrusion process still remains at the moment a challenge, even if the melt

rheology could represent a powerful method to investigate the degree of disaggregation and delamination of clays. However, so far, the major part of the studies concerning dynamic shear measurements was carried out off-line. These last are very sensitive to the morphological status of the nanocomposite melts, but they do not take into account the material processability, which can be instead examined working on-line at high shear rates. This kind of analysis, rarely performed, is crucial for the production of polymer nanocomposites on wide scale particularly by considering that the shear response of layered silicate-based polymer nanocomposites has important consequences on the potential material processability.

By taking into account that any development in this field may be undoubtedly the key to the commercial expansion of LDPE nanocomposites and that the extrusion scale-up is currently the most successful approach for their preparation, in this work chemical and processing parameters were both investigated and evaluated by working with a co-rotating twin screw extruder. With this purpose, by employing an organo-clay already tested for the preparation of polyolefin nanocomposites, the selection of the matrix and compatibilizer was made according to their rheological properties together with a typical functionalization degree (around 1 wt%). The compatibilizer was first melt compounded with the organo-clay in order to prepare a master-batch containing 10 wt% of organo-clay; thus, nanocomposites with two different amounts of clay were prepared by mixing the master-batch with pure LDPE.

Morphology and thermal properties of the master-batch and derived nanocomposites were investigated by x-ray diffraction (XRD), transmission electron microscopy (TEM), differential scanning calorimetry (DSC) and thermo-gravimetric analysis (TGA). The rheological behavior of nanocompounding was studied during the extrusion process with an on-line capillary rheometer to provide a relationship between feed conditions, processing parameters and state of clay dispersion.

Results and discussion

A polyethylene suitable for blow moulding extrusion was selected as matrix (LDPE), together with a maleic anhydride functionalized PE (PE-g-MAH, FD=0,5-1,0 wt%) as compatibilizer. This has a melt viscosity similar to that of the LDPE thus to minimise phase separation risks [31] (see experimental part). The organo-montmorillonite Dellite 72T (D72T) modified by dimethyl dihydrogenated tallow quaternary ammonium was selected as clay [22] and employed for the master-batch preparation. For economic reasons, PE-clay nanocomposites of industrial interest contain no more than 3 wt% of organo-clay and they are preferentially prepared from a master-batch containing a large amount of the additive [32]. This procedure was reported for LDPE nanocomposites prepared for working in an internal mixer [33], where the effect of the shear stress is obviously low. In fact a poor degree of clay exfoliation was observed for the master-batch. In this work a master-batch PE-g-MAH/D72T having a nominal weight ratio of 9:1 was prepared in the extruder with the aim to overstress the effect of clay dispersion. All the nanocomposites were then prepared by diluting the master-batch with LDPE in order to obtain nanocomposites with 1 and 3 wt% of D72T, respectively.

A co-rotating twin screw extruder (Fig. 1) with three kneading zones at different shear intensity was set up for obtaining a decreasing dispersive force along the screw profile which should initially allow the disaggregation of nanoparticles and

successively improve the dispersion of tactoids into discrete monolayers thanks to the distributive mixing action. Moreover the decreasing shear intensity should minimize the polymer degradation.
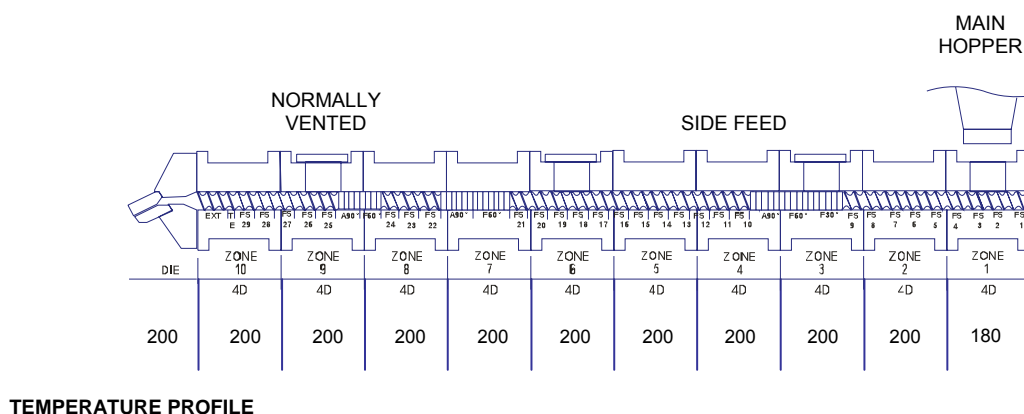

Fig. 1. Screw and temperature profile used for the production of master-batch and nanocomposites

The organo-montmorillonite was added to the molten polymer through a side feeder placed after the first kneading zone. Finally, the effect of processing parameters onto the dispersion degree of clay platelets was studied by varying the screw speed used both for master-batch (50, 75, 90 rpm) and preparation of nanocomposites (90 and 150 rpm).

Preparation and characterization of the master-batch

The XRD spectra of the master-batch extruded at 50, 75 and 90 rpm (Fig. 2) showed, for all the studied screw speeds, a shift of the D72T (001) basal reflection towards smaller angles with respect to the neat organo-clay, thus indicating the occurrence of polymer chains intercalation within the interlayer spacing of clay platelets and the related development of a mixed morphology consisting of intercalated or intercalated/exfoliated structures. This last hypothesis was also confirmed by TEM analysis. As reported in Fig. 3, as an example for the master-batch prepared at 50 rpm, independently of the screw rate, a large number of single clay lamellae was observed as well as tactoids, thus suggesting that at least apparently the morphology was not affected by this processing parameter. Moreover, the lower-magnification TEM micrograph (Fig. 3a) evidenced a certain degree of orientation of lamellae which seemed to be aligned parallel to each other in a well-ordered structure. Therefore a good dispersion of clay layers was assessed for the master-batch thus highlighting the importance of the shear stress [30] for the control of the final morphology.

The DSC of PE-g-MAH showed a broad endothermic peak both in the first and second heating steps with a quite low melting temperature, characteristic of low density PE. The second heating path was used to calculate the crystallinity degree, that was between 11 and 15 % (Tab. 1). The master-batches provided thermogram profiles similar to PE-g-MAH, even if a small decrease of the crystallization temperature (T_c) (~1,5 °C) was observed together with an increase of crystallinity values. Most likely the polyethylene chains that surround the dispersed clay lamellae have a reduced mobility with respect to the far chains, due to the interaction with the clay surface through the polar anhydride groups [34], and as a consequence, the

4

surrounding chains crystallize latter. This is in agreement with results obtained in the case of ternary blends PE/PE-g-MAH/organo-montmorillonite [35, 36].
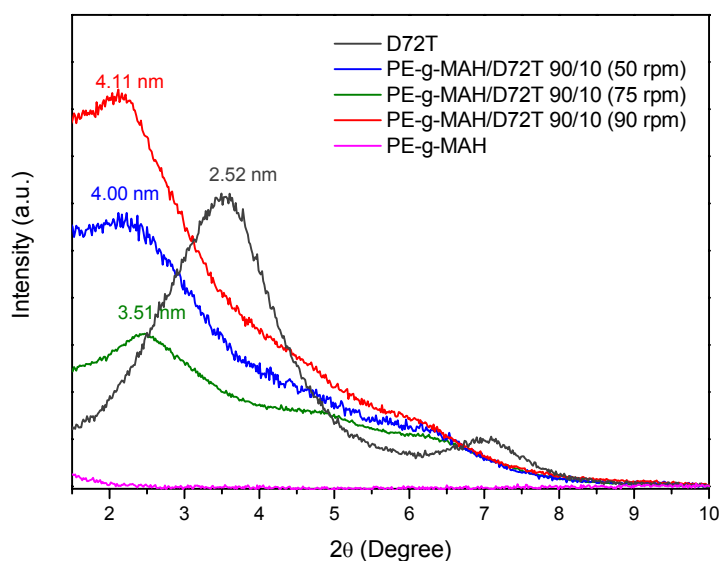

Fig. 2. Comparison among the XRD spectra of the master-batch extruded at 50, 75 and 90 rpm and of neat components in the 1,5-10° region.
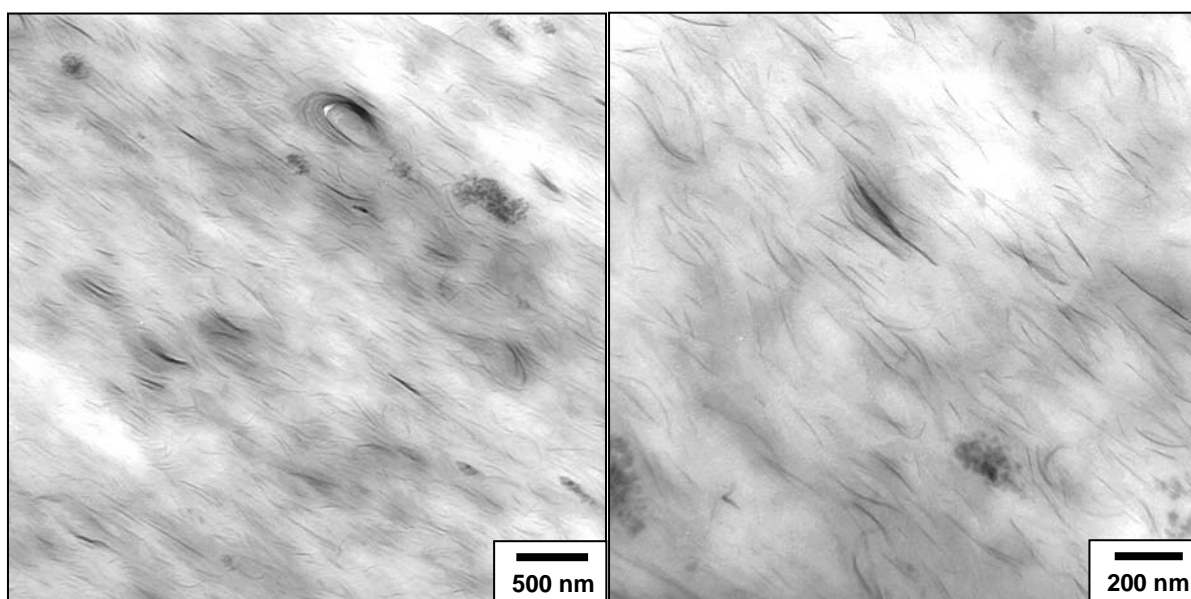

Fig. 3. TEM micrographs of ultrathin sections of PE-g-MAH/D72T master-batch (50 rpm)

From XRD spectra of PE-g-MAH and master-batches (Fig. 4), in the region of reflections of the polyethylene crystal structure (10-40° of 2θ) [38], it was possible to evaluate a 12% crystallinity degree [39]. The reflection at 20,8° increased in intensity with respect to the reflection at 23,1° for all the master-batches compared with the pure PE-g-MAH (Fig. 4) and it also grew by increasing the screw speed. This evidence indicates a raise of the crystal orientation along a preferential direction [40],

5

which could be a consequence of the orientation of the clay platelets highlighted by TEM analysis.

Tab. 1. DSC data of PE-g-MAH and PE-g-MAH/D72T 90/9 master-batch extruded at 50, 75 and 90 rpm.

Sample	T_c (°C)	T_m (°C)	χ_c (%)*
PE-g-MAH	47,2	70,4	11
PE-g-MAH/D72T 90/10 (50 rpm)	45,7	70,5	14
PE-g-MAH/D72T 90/10 (75 rpm)	45,6	69,8	15
PE-g-MAH/D72T 90/10 (90 rpm)	45,6	70,2	14

*Calculated as follows: $\chi_c = \Delta H_m / (1-x) \Delta H_m^0$, where ΔH_m is the experimental melting enthalpy, *(1-x)* is the polyethylene fraction by weight in the composite and ΔH_m^0 is the melting enthalpy of infinite polyethylene crystal (293 J/g) [37].
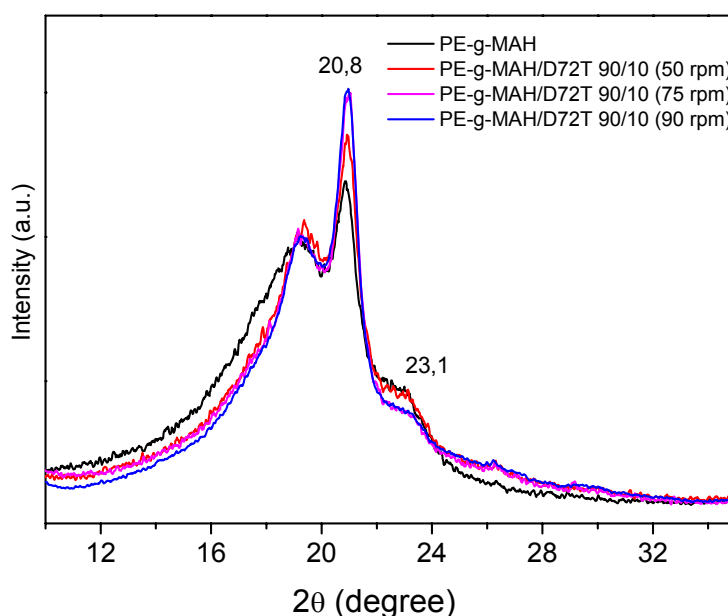

Fig. 4. XRD plots of master-batch extruded at 50, 75 and 90 rpm. Diffractograms were normalised at 19,2° for comparison purpose.

Tab. 2. TGA data of PE-g-MAH and PE-g-MAH/D72T 90/10 master-batch extruded at 50, 75 and 90 rpm

Sample	$T_{10\%}$ (°C)	$\Delta T_{10\%}$ (°C)	$T_{50\%}$ (°C)	$\Delta T_{50\%}$ (°C)
PE-g-MAH	351,3	–	401,8	–
PE-g-MAH/D72T 90/10 (50 rpm)	432,7	81,4	467,2	65,4
PE-g-MAH/D72T 90/10 (75 rpm)	433,0	81,7	468,0	66,2
PE-g-MAH/D72T 90/10 (90 rpm)	433,0	81,7	469,3	67,5

6

The TGA carried out under air flow of the master-batches (Fig. 5) showed a significant thermal stabilization (~60 °C) (Tab. 2) with respect to the pure PE-g-MAH. Moreover, the degradation of master-batches occurred in a single sharp step with middle temperature point at 460 °C, while starting PE-g-MAH degraded in a wide temperature range with two main shared processes having middle temperature points at 403 and 530 °C, respectively.
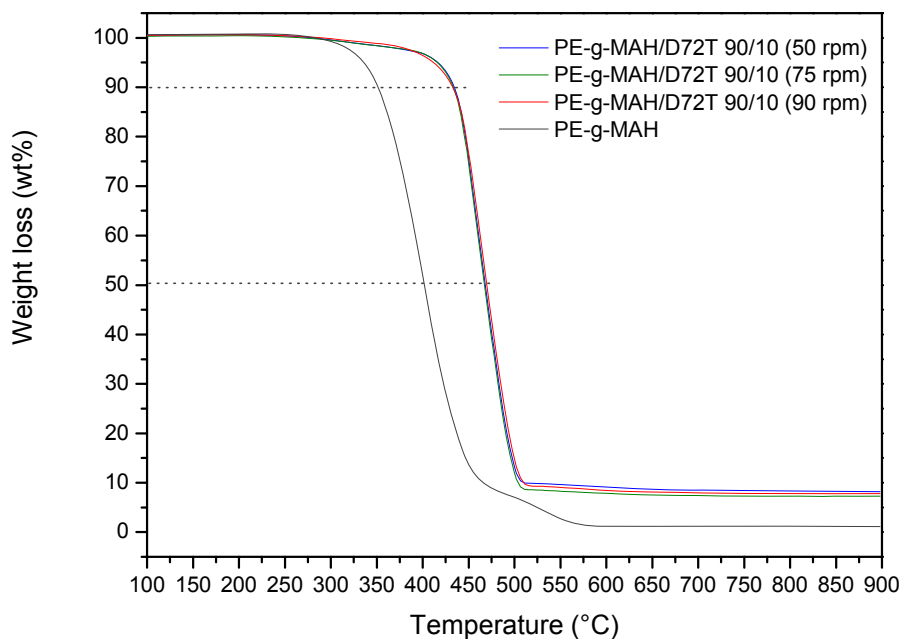

Fig. 5. TGA analysis under air flow of PE-g-MAH and master-batch extruded at 50, 75 and 90 rpm.

Preparation and characterization of the nanocomposites

The LDPE/PE-g-MAH/D72T 90/9/1 and 70/27/3 nanocomposites with 1 and 3 wt% of D72T respectively (as confirmed by EDXS analysis) were prepared by melt compounding the master-batch (50 rpm) with pure LDPE at 90 and 150 rpm.

Independently of the composition, the broad XRD (001) peak in the master-batch due to D72T shifted to lower angles and its intensity decreased in the nanocomposites indicating the further increase of the *d*-spacing and most likely the promotion of clay exfoliation (Fig. 6). The increase of the screw speed from 90 to 150 rpm did not cause appreciable changes of the (001) peak for the nanocomposite 1 wt%. On the contrary, a significant decrease of D72T (001) basal reflection intensity was observed for the nanocomposite 3 wt% going from the lower to the higher rate, suggesting that the higher speed overcame the extra-viscosity due to the increased amount of clay favouring its dispersion/exfoliation. On the whole the XRD spectra evidenced the presence of a weak tail of the D72T (001) peak around the limit of detection of the instrument. This could be apparently associated with the formation of exfoliated nanocomposites or it may be due to a concentration effect. However, TEM micrographs showed that some ordered stacks, having a quite high value of the distance between lamellae, still persisted.

7

TEM micrographs of nanocomposites with 1 and 3 wt% of D72T (Fig. 7 and Fig. 8, respectively) confirmed the XRD results: both samples resulted mainly composed of exfoliated layers, even if a very small amount of intercalated tactoids still seemed to persist.
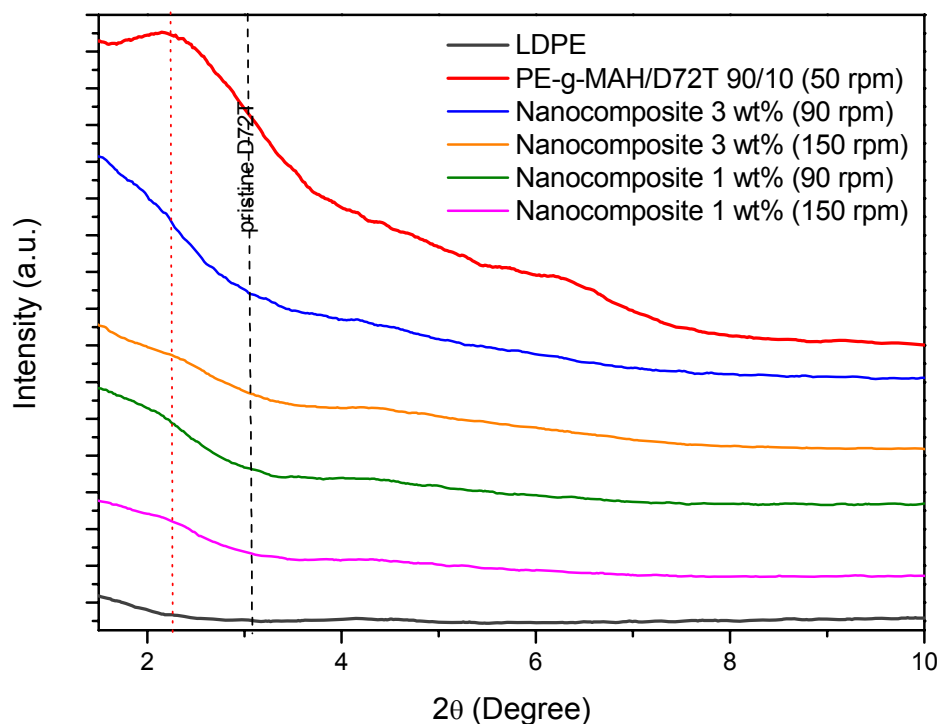

Fig. 6. XRD patterns of nanocomposites 1 and 3 wt% D72T at different screw speeds and same feed rate.

Moreover, as already noted for the master-batch, the process of compounding/extrusion was responsible for a significant effect of *organo-clay platelet alignment* along a preferential direction for all the samples, as shown in particular for the nanocomposite 3 wt% prepared at 150 rpm (Fig. 8 c,d).

The complementary role of the shear stress and interface interactions is evident when the effect of the different screw speed rates is compared for both the nanocomposites. In fact, no significant morphological differences were observed for the nanocomposite 1 wt% extruded at 90 and 150 rpm because the interface interactions allowed to obtain good dispersion even at low shear stress. Instead, when the clay amount increased up to 3 wt%, a higher energy amount should be supplied (higher shear stress) to achieve the separation of all the platelets (see the better morphology of nanocomposite 3 wt% 150 rpm *vs.* 90 rpm).

The DSC analysis of nanocomposites and of corresponding LDPE/PE-g-MAH blend matrices, taken as reference, was performed. The addition of 1 wt% organo-clay did not significantly affect the thermal properties of LDPE: both melting (T_m) and crystallization (T_c) temperature seemed unchanged and only a very slight increase of crystallinity was observed for both the screw speeds (Tab. 3).
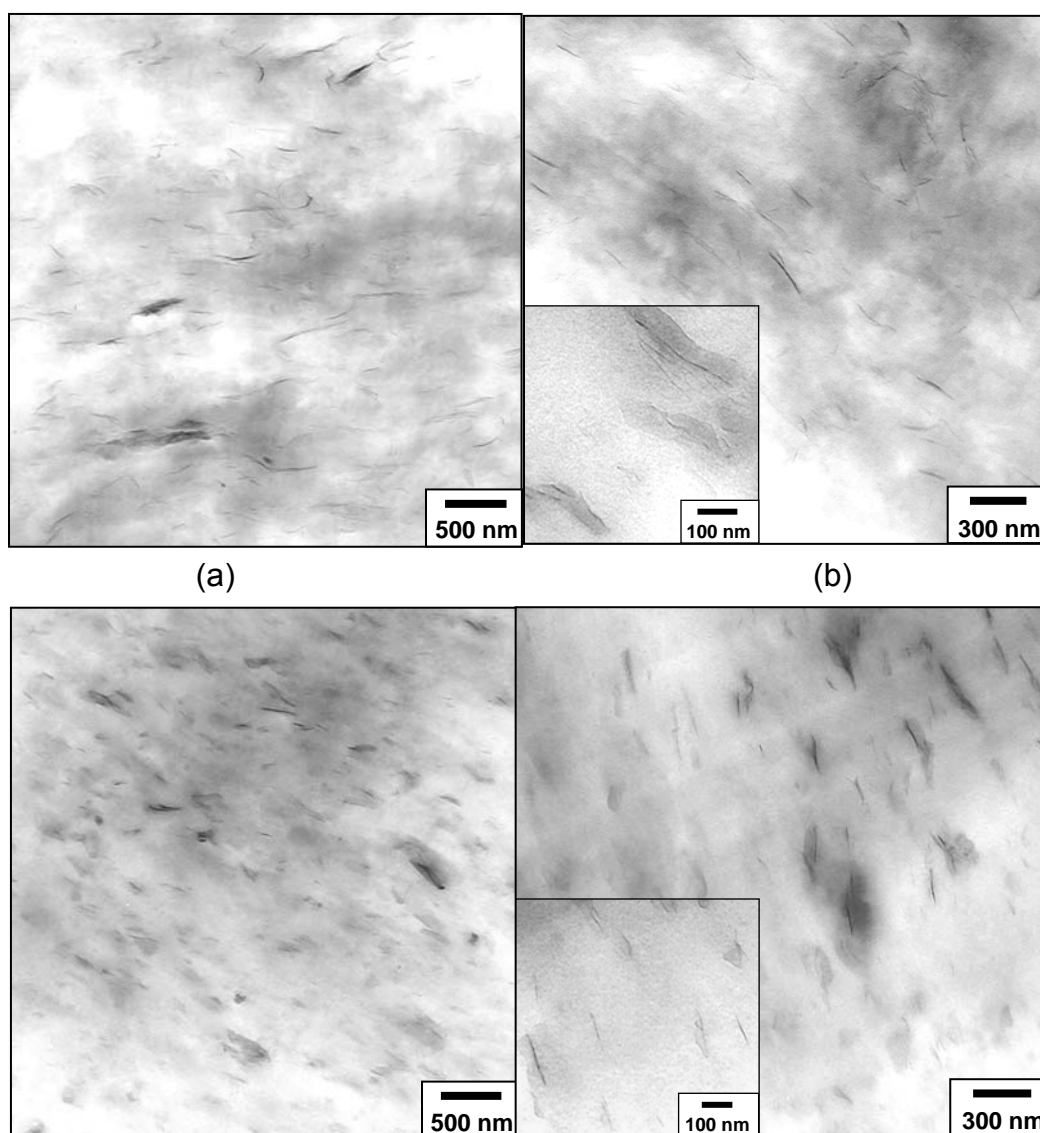
Fig. 7. TEM micrographs of ultrathin sections of nanocomposite 1 wt% extruded at different screw speeds: (a,b) 90 rpm; (c,d) 150 rpm.

Tab. 3. DSC data of LDPE/PE-g-MAH blends and LDPE/PE-g-MAH/D72T nanocomposites.

Sample	T_c (°C)	T_m (°C)	χ_c (%)*
LDPE/PE-g-MAH (90/9)	86,5	111,9	37
LDPE/PE-g-MAH (70/27)	86,3	110,6	32
Nanocomposite 1 wt% (90 rpm)	87,2	112,6	38
Nanocomposite 1 wt% (150 rpm)	87,5	111,8	38
Nanocomposite 3 wt% (90 rpm)	84,9	112,6	34
Nanocomposite 3 wt% (150 rpm)	86,0	111,5	34

*Calculated as follows: $\chi_c = \Delta H_m/(1-x)\Delta H_m^0$, where ΔH_m is the experimental melting enthalpy, *(1-x)* is the polyethylene fraction by weight in the composite and ΔH_m^0 is the melting enthalpy of infinite polyethylene crystal (293 J/g) [37].

9

In the case of nanocomposites containing 3 wt% organo-clay, it was observed a more significant increase of both T_m and crystallinity degree (χ_c) with respect to the corresponding LDPE/PE-g-MAH (70/27) matrix, independently of the screw rate as already mentioned for the master-batch.
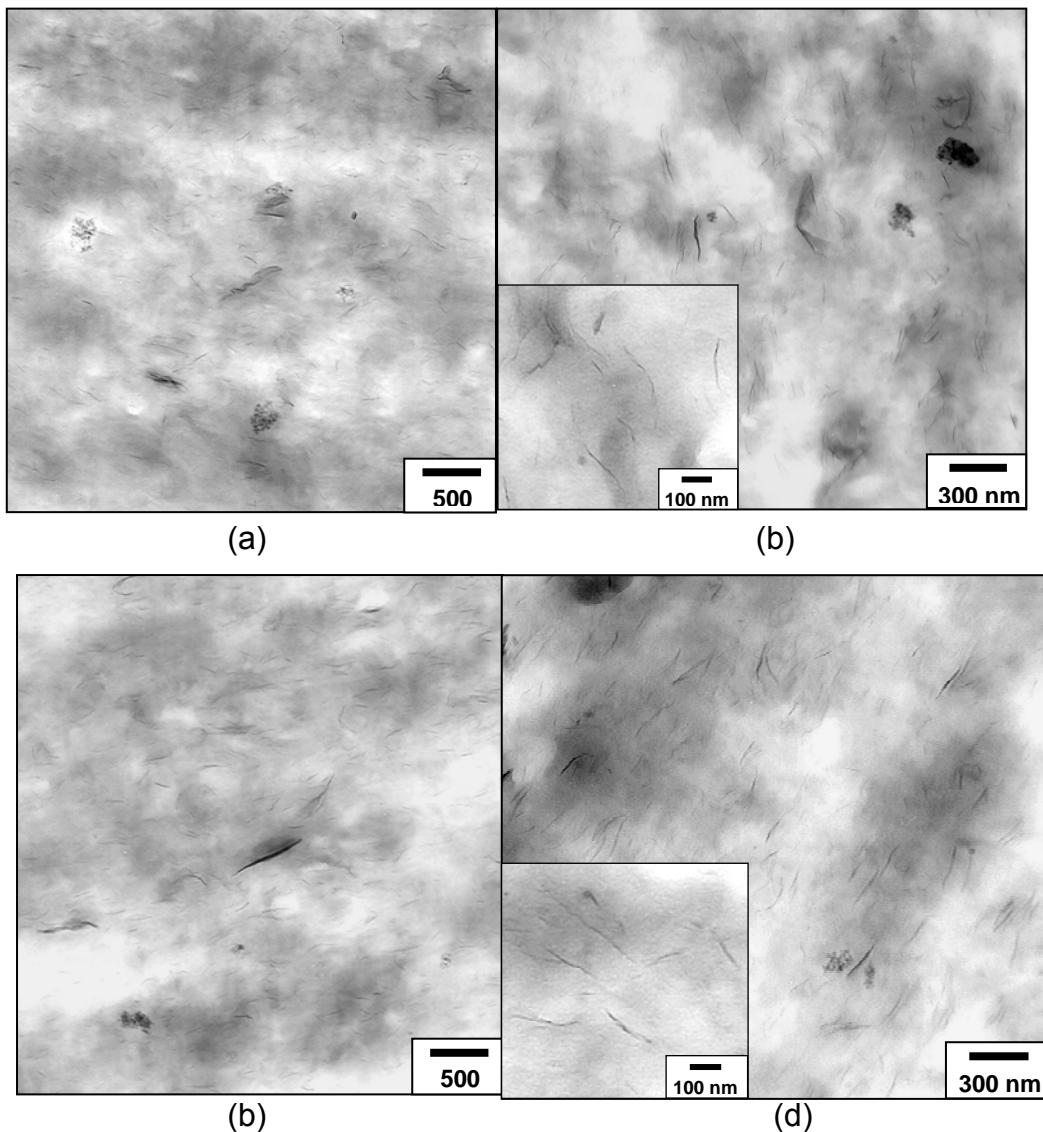

Fig. 8. TEM micrographs of ultrathin sections of nanocomposite 3 wt% extruded at different screw speeds: (a,b) 90 rpm; (c,d) 150 rpm

The XRD analysis of nanocomposites 3 wt% showed a decrease of the relative intensity of the (110) diffraction peak of polyethylene with respect to the (200) peak by addition of the clay (Fig. 9) as indication of molecular axis orientation [40].

The mathematical deconvolution [39] of the XRD pattern profile, with Gaussian-shape curves, allowed to calculate the $I_{(110)}/I_{(200)}$ ratio (Tab. 4). The LDPE $I_{(110)}/I_{(200)}$ ratio is in agreement with the literature value found for unoriented PE specimens [41], while for nanocomposites 3 wt% a lower value was found. Only a slight decrease was instead observed for nanocomposites 1 wt%. The decrease of the $I_{(110)}/I_{(200)}$ ratio as well as the slight increase of the crystallinity degree by DSC for nanocomposites 3 wt% could be tentatively related with the orientation of both macromolecules and

10

lamellae (as shown by TEM pictures) [42] by the extrusion process. In this way the orientation of macromolecules could have promoted the crystallization favouring the crystallinity increase as already reported in literature [43] (Fig. 10). The lower effect observed for nanocomposites 1 wt% (lower orientation and lower crystallinity increase) is probably due to the lower amount of lamellae.
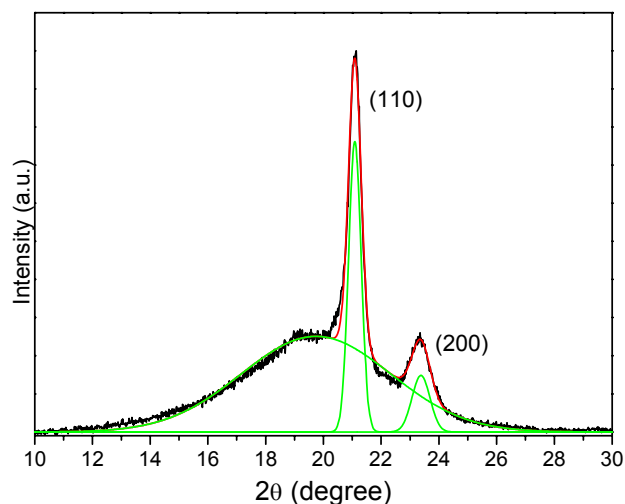

Fig. 9. XRD spectrum of nanocomposite 3 wt% (90 rpm) in the 10-30° diffraction range (black), Gaussian peaks for the amorphous halo and the polyethylene crystal reflections as obtained by the deconvolution procedure (green) and sum of the three deconvolution peaks (red).
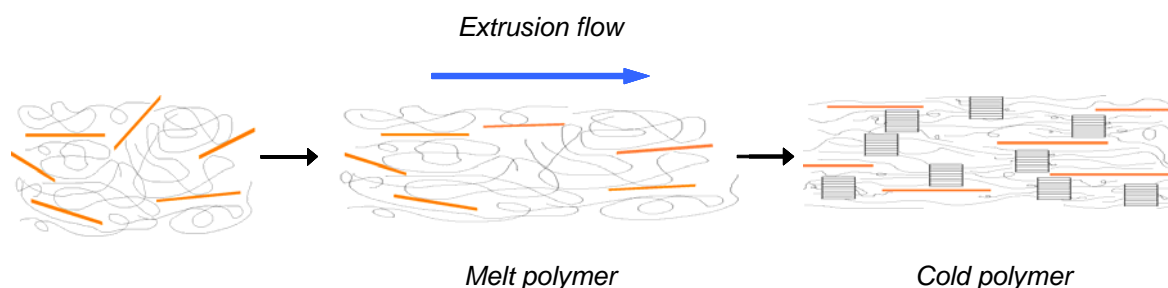

Fig. 10. Representation of the effect of extrusion flow on the process of macromolecules and clay lamellae orientation in the polymer melt and crystallization of oriented macromolecular chains.

The thermal stability of LDPE/PE-g-MAH blends and of their nanocomposites with D72T was tested by TGA under air flow. Both nanocomposites started to degrade at higher temperature than pure polymer blends thus evidencing enhanced stability. For the nanocomposites 1 wt% the decomposition temperature $T_{10\%}$, which is measured at the point of 10 wt% mass loss, shifted by about 20 °C compared with the pure matrix (LDPE/PE-g-MAH 90/9) (Tab. 5). The $T_{10\%}$ still increased by about 30-40 °C on increasing the master-batch loading (nanocomposites 3 wt%). The same trend was observed for $T_{50\%}$ which also increased significantly for both the nanocomposites.

11

Tab. 4. Ratio between XRD d(110) and d(200) intensity peaks of orthorhombic polyethylene polymorph for pure LDPE and nanocomposites with different content of D72T obtained at different screw rate.

Sample	$I_{(110)}/I_{(200)}$
LDPE	4,0
Nanocomposite 1 wt% (90 rpm)	3,9
Nanocomposite 1 wt% (150 rpm)	3,9
Nanocomposite 3 wt% (90 rpm)	3,6
Nanocomposite 3 wt% (150 rpm)	3,4

Tab. 5. TGA data of LDPE/PE-g-MAH blends and LDPE/PE-g-MAH/D72T nanocomposites.

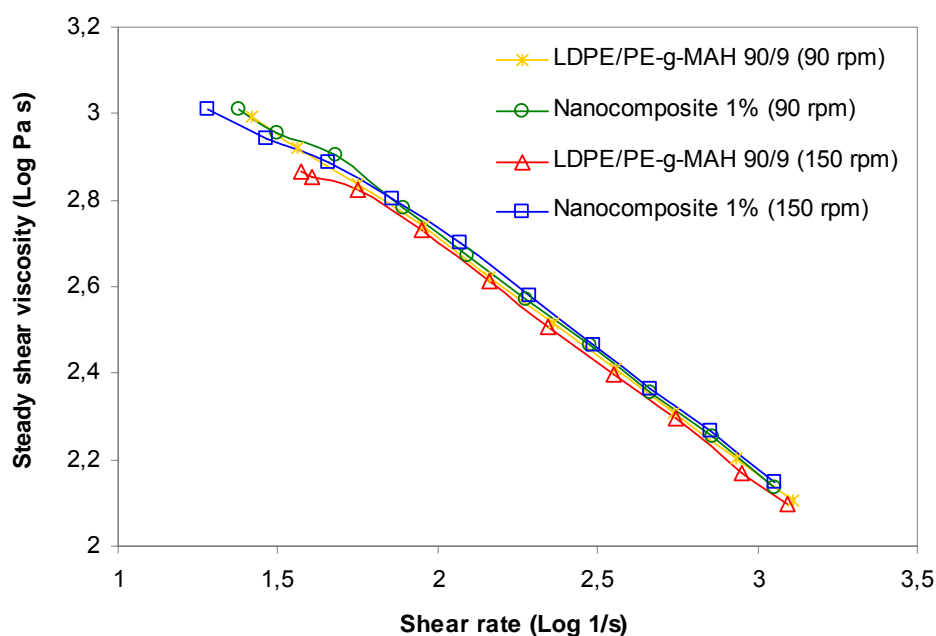| Sample	$T_{10\%}$ (°C)	$\Delta T_{10\%}$ (°C)	$T_{50\%}$ (°C)	$\Delta T_{50\%}$ (°C)
LDPE/PE-g-MAH (90/9)	360,8	–	397,4	–
LDPE/PE-g-MAH (70/27)	371,6	–	404,8	–
Nanocomposite 1 wt% (90 rpm)	384,6	23,8	441,4	44,0
Nanocomposite 1 wt% (150 rpm)	381,7	20,9	450,8	53,4
Nanocomposite 3 wt% (90 rpm)	401,4	29,8	459,4	54,6
Nanocomposite 3 wt% (150 rpm)	412,3	40,7	465,2	60,4

Fig. 11. Steady shear viscosity *vs.* shear rate of nanocomposite 1 wt% and LDPE/PE-g-MAH 90/9 blend.

12

On-line capillary rheometer measurements carried out during the extrusion process did not show any significant difference in the steady shear viscosity behavior *vs.* shear rate at any screw speed for all the nanocomposites prepared with respect to their reference matrices (see for example Fig. 11). Most likely silicate layers were strongly oriented towards the flow direction and for this reason the shear thinning behavior was principally dominated by the matrix properties [44].
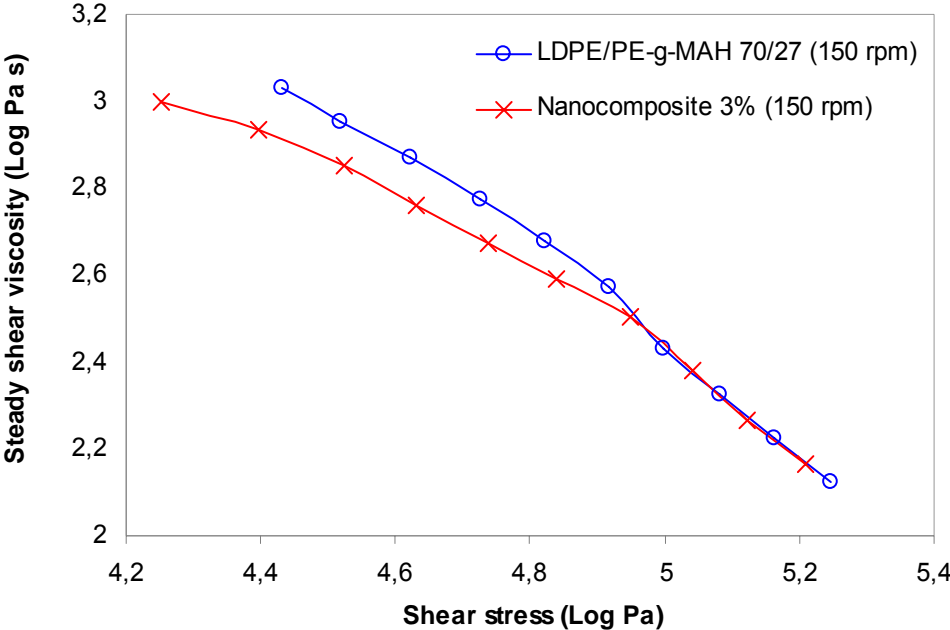

Fig. 12. Steady shear viscosity *vs.* shear stress of nanocomposite 3 wt% and LDPE/PE-g-MAH 70/27 blend both melt compounded at 150 rpm.
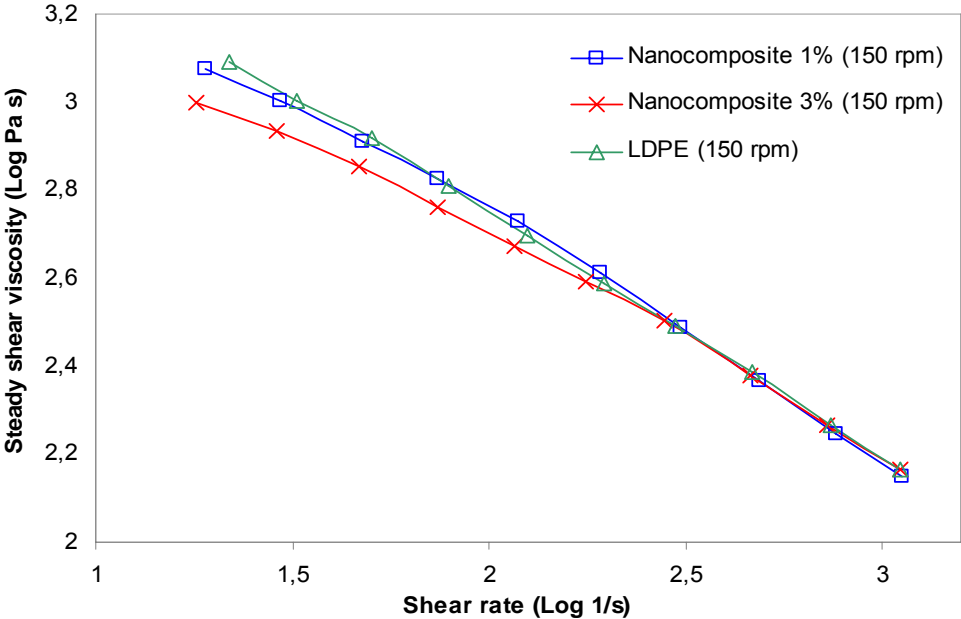

Fig. 13. Comparison between flow curves of nanocomposites and pure LDPE.

13

In the graphic of shear viscosity *vs.* shear stress, which is much more sensible to the composite structure, it was possible to observe that at low shear stress, for the nanocomposite prepared by adding the highest organo-clay amount (3 wt%) and at the highest screw speed (150 rpm), the shear viscosity was lower than that of the corresponding matrix (LDPE/PE-g-MAH 70/27) (Fig. 12). This effect could be explained on the basis of a higher degree of organo-clay platelets alignment in agreement with TEM analysis.

These results suggested that at high shear rate the reinforcing elements into the composite were oriented in the flow direction so that the processability of LDPE was not compromised by the presence of the filler (Fig. 13).

Finally, the on-line rheology evidenced that high shear stresses were exerted during the measurements both for master-batch and nanocomposites (44÷244 kPa for the master-batch and 25÷160 kPa for the nanocomposites) which were most likely responsible of particles breakup and ultimately improved clay platelet exfoliation.

Conclusions

The chemical and processing parameters selected on the basis of literature information were suitable to get well dispersed LDPE/organo-montmorillonite nanocomposites. A two step process consisting in the preparation of a PE-g-MAH/clay 90/10 master-batch, then used for getting LDPE nanocomposites at different composition, was successfully scaled up in a twin screw extruder. Herein both the interactions at the polymer/clay interface and the shear stress in the extruder acted for establishing the final nanocomposite morphology. In particular the right balance between dispersive and distributive actions by the screw profile allowed to optimize the morphology both of master-batch and nanocomposites. Indeed, a good dispersion of clay layers was already assessed in the master-batch thus highlighting the importance of the shear stress for dispersing, intercalating and exfoliating lamellae after the proper interface interactions are provided. A further improvement of the dispersion degree was observed during the second processing step, since the melt viscosity of the two polymer components was accurately selected with the aim to improve their compatibility. The combination of TEM, XRD and DSC analyses allowed to assess that both lamellae and macromolecules were oriented by the extrusion process in particular in the 3 wt% nanocomposites thus influencing their rheological and thermal properties.

Experimental part

Materials

Low density polyethylene (LDPE) Riblene FL34 with a density of 0,924 g/cm^3 and melt flow index of 2,1 g/10 min (190 °C, 2.16 Kg) was purchased from Polimeri Europa. The organo-montmorillonite Dellite 72T (abbreviation D72T) modified by dimethyl dihydrogenated tallow quaternary ammonium salt was supplied by Laviosa Chimica Mineraria. Maleic anhydride modified polyethylene UL EP Compoline® by Auserpolimeri (abbreviation PE–g-MAH) having a melt flow index of 2,5 g/10 min (190°C, 2,16 Kg) and an amount of succinic anhydride grafted groups of 0,5-1,0 wt% was selected as compatibilizer.

14

Nanocomposites were obtained by a two step process. In the first step a master-batch was prepared by mixing in the extruder the compatibilizer and the organo-clay in nominal proportion by weight of 90/10. In agreement, the amount of organo-clay, checked by TGA, with respect to the amount of composite, resulted to be 10±1 wt%. In the second step the master-batch was blended with LDPE and nanocomposites having a relative weight proportion of 90/9/1 and 70/27/3 (LDPE/PE-g-MA/D72T) respectively were prepared. LDPE/PE-g-MAH/D72T nanocomposites were prepared via direct melt intercalation in a pilot-scale intermeshing co-rotating twin screw pilot extruder (Thermo-Haake) with following characteristics: barrel length of 960 mm, screw diameter of 24 mm and length-to-diameter ratio (L/D) of 40. The screw profile is composed of 10 zones (each zone has L/D=4) with 3 interposed kneading sections, the first kneading section started at the third zone and it was made up of 16 kneading discs, the second started at the seventh zone and it was made up of 13 kneading discs, while the last started at the eighth zone and it was made up of 8 kneading discs. In the ninth zone there was a vent port which was kept open during the extrusion process. A gear pump that conveys the melt mass to a rod capillary die was connected to the tenth zone, between the extruder and the die. A capillary die with diameter of 3 mm and L/D=20 was used for master-batch preparation, while capillaries dies with diameter of 1 mm were used for rheology measurements and nanocomposites production. The instrument has the possibility of conducting on-line rheological tests and for this reason it is provided with different types of capillary dies. Then, master-batch and nanocomposites samples were taken at the die exit after having reached steady-state extrusion conditions, solidified in a water bath and pelletized with standard pelletizing machine. For the master-batch preparation, the compatibilizer PE-g-MAH was fed in the main hopper and the organo-clay D72T was introduced through the side feeder (after polymer melting). After several trials, the barrel temperature was set, for all the experiments, at 180 °C for the first zone and at 200 °C for all the others, whereas the fed rate of PE-g-MAH was 0,9 kg/h and the clay was fed at the rate of 0,1 kg/h. Screw rotation speed was 50, 75 or 90 rpm. The LDPE was extruded and pelletized before blending with master-batch to obtain similar shape and size and thus to allow good mixing of the pellets. The process was carried out at 90 rpm, the fed rate was 1,8 kg/h and the barrel temperature was fixed at 190 °C for the first zone and 220 °C for all the others. Nanocomposites were instead prepared by mechanical mixing of LDPE and master-batch at room temperature which were later introduced in the hopper and fed at the rate of 1 kg/h. After several trials, the barrel temperature was fixed for the all experiments at 180 °C for the first zone and at 200 °C for all the others. Screw speed was 90 and 150 rpm. LDPE, PE-g-MAH and LDPE/PE-g-MAH blends with 90/9 and 70/27 weight ratio were also extruded, pelletized and used as reference materials.

Characterizations

Pure polymers, blends, master-batch and nanocomposites specimens of 2×1×0.2 cm were prepared for XRD and TEM analyses by compression moulding in a plane plates hydraulic press (Collin P200M) with the following thermal program: 1st step T=200 °C (pre-heated), for 600 s at P=0 bar; 2nd step T=200 °C, for 60 s at P=1 bar; 3rd step T=200 °C for 60 s at P=2 bar; 4th step T=200 °C for 60 s at P=3 bar; 5th step quenching with cassette cooled by water for 120 s at P=3 bar.

X-ray diffraction (XRD) patterns of D72T, PE-g-MAH/D72T master-batch and LDPE/PE-g-MAH/D72T nanocomposites were recorded at room temperature by using a Siemens Kristalloflex 810 diffractometer (Cu K$_\alpha$ radiation, λ=0,15406 nm) in the 1,5–40° 2θ region at the scanning rate of 0,016 degree/s. Morphology of master-batches and nanocomposites was investigated also by TEM with a Zeiss EM 900 microscope applying an accelerating voltage of 80 kV. Ultrathin sections (about 50 nm thick) of sample plaques were obtained by using a Leica EM FCS cryoultramicrotome equipped with a diamond knife (sample temperature: -145 °C; knife temperature: -60 °C). The energy dispersive X-ray spectroscopy (EDXS) of the 3 wt% nanocomposites was performed with a Jeol JSM model T-300 instrument equipped with an Oxford X-ray energy dispersive spectrometer microprobe was performed on cryogenic fractured samples. The observed Si atomic percentage agreed with the value expected by the nominal amount of fed D72T.

Thermo-gravimetric analysis (TGA) was performed with a Mettler Toledo Stare System TGA/SDTA 851^e Module. Samples (5-10 mg) were placed in an alumina sample pan and runs were carried out at a standard rate of 10 °C/min from 25 to 900 °C under air flow (60 ml/min). A Perkin-Elmer DSC-7 differential scanning calorimeter thermal analyzer equipped with a CCA/liquid nitrogen cooling unit was used for DSC analyses. Thermal scanning's of melting-crystallization-melting (0-200 °C at 20 °C/min) were performed under nitrogen atmosphere after the instrument calibration carried out by using melting temperatures and enthalpies of indium (T$_m$=156,60 °C; ΔH$_m$=28,47 J/°C) and zinc (T$_m$=419,47 °C) as standards.

Steady shear viscosities of LDPE/PE-g-MAH/D72T nanocomposites were measured at 200 °C by using the on-line capillary rheometer (OLR). An exact flow of melt polymer was conveyed by melt pump in a capillary at 200 °C. The true shear rate, true shear stress and true steady shear viscosity were measured with two capillaries for rheological measurements with diameter of 1mm and length of 10 and 30 mm respectively, varying the melt pump speed to change shear rate. The measurements were performed using two capillaries with diameter of 1mm and length 10 and 30 mm respectively necessary to remove the entrance and exit pressure drops from the measured signal leading to true shear stress values. The range of true shear rate investigated was approximately 16-900 s^{-1}. Strain rates were controlled by a gear pump and chosen capillary die geometry. The apparent shear rate of melt polymer into the capillary was calculated using the pump volume and the selected geometry of the die with the following formula (eq. 1):

$$\dot{\gamma}_{app} = \frac{4 \cdot Q}{\pi \cdot r^3} \tag{1}$$

where $\dot{\gamma}_{app}$ is the shear rate (s^{-1}), Q is the volume stream (m^3/s), r is the radius rod capillary (m). While the apparent shear stress was calculated as it follows (eq. 2):

$$\tau_{app} = \frac{r \cdot \Delta p}{2l} \tag{2}$$

where l is the capillary length (m), Δp is the pressure drop (Pa) which was measured by a pressure transducer.

The data directly obtained by the OLR are apparent values (shear rate, shear stress and viscosity), as they inherit some faults caused by the measurement principle.

Therefore the shear stress data were corrected with the Bagley correction whereas for shear rate was applied the Weissenberg–Rabinowitsch equation (eq. 3):

$$\dot{\gamma} = \frac{\dot{\gamma}_{app}}{4} \cdot \left(3 + \frac{d \ln \dot{\gamma}_{app}}{d \ln \tau} \right) \text{ (for the rod capillary die)} \tag{3}$$

Finally the true steady shear viscosity (η) (Pa s) was calculated with the following formula (eq. 4):

$$\eta = \frac{\tau}{\dot{\gamma}} \tag{4}$$

References

[1] Százdi, L.; Pozsgay, A.; Pukánszky, B. *Eur. Polym. J.* **2007**, *43*, 345.
[2] Ray, S.; Easteal, A. J. *Mater. Manuf. Processes* **2007**, *22*, 741.
[3] Okamoto, M. *Int. Polym. Proc.* **2006**, *21*, 487.
[4] Okamoto, M. *Mater. Sci. Technol.* **2006**, *22*, 756.
[5] Nguyen, Q. T.; Baird, D. G. *Adv. Polym. Tech.* **2006**, *25*, 270.
[6] Ray, S. S.; Okamoto, M. *Prog. Polym. Sci.* **2003**, *28*, 1539.
[7] Sirousazar, M.; Yari, M.; Achachlouei, B. F.; Arsalani, J.; Mansoori, Y. *e-Polymers* **2007**, no. 027
[8] Ray, S.; Quek, S. Y.; Easteal, A.; Chen, X. D. *Int. J. Food Eng.* **2006**, *2*, article 5.
[9] Mainil, M.; Alexandre, M.; Monteverde, F.; Dubois, P. *J. Nanosci. Nanotech.* **2006**, *6*, 337.
[10] Osman, M. A.; Rupp, J. E. P.; Suter, U. W. *Polymer* **2005**, *46*, 8202.
[11] Shah, R. K.; Paul, D. R. *Polymer* **2006**, *47*, 4075.
[12] Zhang, J.; Wilkie, C. A. *Polym. Deg. Stab.* **2003**, *80*, 163.
[13] Su, S.; Jiang, D. D.; , Wilkie, C. A. *Polym. Deg. Stab.* **2004**, *83*, 321.
[14] Tzavalas, S.; Macchiarola, K.; Gregoriou, V. G. *J. Polym. Sci., Part B: Polym. Phys.* **2006**, *44*, 914.
[15] Osman, M. A.; Rupp, J. E. P.; Suter, U. W. *Polymer* **2005**, *46*, 1653.
[16] Gopakumar, T. G.; Lee, J. A.; Kontopoulou M.; Parent, J. S. *Polymer* **2002**, *43*, 5483.
[17] Durmus, A.; Kasgoz, A.; Macosko, C. W. *Polymer* **2007**, *48*, 4492.
[18] Wang K. H.; Choi, M. H.; Koo, C. M.; Choi, Y. S.; Chung, I. J. *Polymer* **2001**, *42*, 9819.
[19] Hotta, S.; Paul, D. R. *Polymer* **2004**, *45*, 7639.
[20] Liang, G.; Xu, J.; Bao, S.; Xu, W. *J. Appl. Pol. Sci.* **2004**, *91*, 3974.
[21] Passaglia, E.; Sulcis, R.; Ciardelli, F.; Malvaldi, M.; Narducci, P. *Polym. Int.* **2005**, *54*, 1549.
[22] Passaglia, E.; Bertoldo, M.; Ceriegi, S.; Sulcis, R..Narducci, P.; Conzatti. L. *J. Nanosci. Nanotechnol.* **2008**, *8*, 1690.

[23] Koo, C. M.; Ham, H. T.; Kim, S. O.; Wang, K. H.; Chung, I. J. *Macromolecules* **2002**, *35*, 5116.

[24] Yang, K.; Ozisik, R. *Polymer* **2006**, *47*, 2849.

[25] Perrin-Sarazin, F.; Ton-That, M. T.; Bureau, M. N.; Denault, J. *Polymer* **2005**, *45*, 11624.

[26] Cho, J. W.; Paul, D. R. *Polymer* **2001**, *42*, 1083.

[27] Lertwimolnun, W.; Vergnes, B. *Polymer* **2005**, *46*, 3462.

[28] Hunter, H. D.; Chang, D. L.; Kim, S.; White, J. L.; Cho, J. W.;. Paul, D. R. *Polymer* **2001**, *42*, 9513.

[29] Lertwimolnun, W.; Vergnes, B. *Pol. Eng. Sci.* **2006**, *46*, 314.

[30] Dennis, H. R.; Hunter, H. D.; Chang, D. L.; Kim, S.; White, J. L.; Cho, J. W.; Paul, D. R. *Polymer* **2001**, *42*, 9513.

[31] Harrats, C.; Groeninckx, G. *"Modification and Blending of Synthetic and Natural Macromolecules",* in NATO Science Series II: Mathematics, Physics and Chemistry, 155-199, **2004**.

[32] Murphy, J. *"Additives for Plastics Handbook"*, 2nd edition, Elsevier, Oxford **2001**.

[33] Morawiec, J.; Pawlak, A.; Slouf, M.; Galeski, A.; Piorkowska, E.; Krasnikowa, N. *Eur. Polym. J.* **2005**, *41*, 115.

[36] Passaglia, E.; Bertoldo, M.; Ciardelli, F.; Prevosto, D.; Lucchesi, M. *Eur. Polym. J.* **2008**, *44*, 1296

[34] Xu, J-T.; Wang, Q.; Fan, Z-Q. *Eur. Polym. J.* **2005**, *41*, 3011.

[35] Golebiewski, J.; Rozanski, A.; Dzwonkowski, J.; Galeski, A. *Eur. Polym. J.* **2008**, *44*, 270.

[37] Wunerlich, B.; Czornyi, G. *Macromolecules* **1977**, *10*, 906.

[38] Bunn, C. W. *Trans. Faraday Soc.* **1939**, 35, 482.

[39] Kavesh, S.; Schults, J. M. *Polym. Eng. Sci.* **1969**, 9, 5.

[40] Galeski, A. *Prog. Polym. Sci.* **2003**, *28*, 1643.

[41] Famulari, A.; Arosio, P.; Filippi, S.; Marazzato, C.; Magagnini, P.; Minkova, L.; Meille, S. V. *J. Macromol. Sci.* **2007**, *46*, 355

[42] Sterzynski, T. *J. Macromol. Sci., Phys.* **1988**, *27*, 369.

[43] Psarski, M.; Piorkowska, E.; Galeski, A. *Macromolecules* **2000**, *33*, 916.

[44] Fornes, T. D.; Yoon, P. J.; Keskkula, H.; Paul, D. R. *Polymer* **2001**, *42*, 9929.